

Understanding the Contributions of Microscopic Heat Transfer to Thermal Conductivities of Liquid Aldehydes and Ketones by Molecular Dynamics Simulation

Fan Yang, Haixia Lu, Wanqiang Liu,* and Hu Zhou*



Cite This: <https://dx.doi.org/10.1021/acs.jcim.0c00184>



Read Online

ACCESS |



Metrics & More

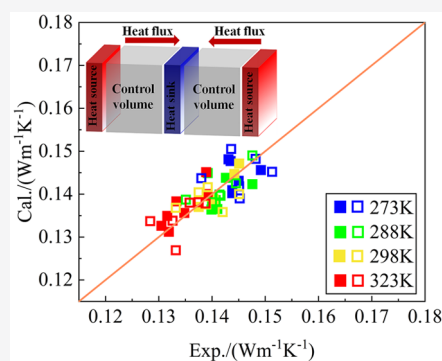


Article Recommendations



Supporting Information

ABSTRACT: Thermal conductivity measurements for organic molecules are difficult and time-consuming. In this study, the thermal conduction of liquid aldehydes and ketones was simulated using nonequilibrium molecular dynamics, and the thermal conductivity at different temperatures was calculated. The deviation between the calculated values and the experimental data of thermal conductivity is less than 4.86%. By decomposing the heat flux, we found that thermal energy is primarily transferred through the torsion angle, angle bending, Coulomb interaction, and kinetic energy in the liquid state. Moreover, as the molecular chain grows, the thermal energy transmitted through the nonbonded interaction decreases, and the thermal energy transmitted through the intramolecular bonded interaction increases, which indicates a significant relationship between the mechanism of heat transfer and the molecular structure. Using molecular dynamics simulation, this research offers a preliminary understanding of the contributions of microscopic heat transfer to the thermal conductivities of liquid aldehydes and ketones.



1. INTRODUCTION

Thermal conductivity is a basic datum used in many fields.¹ Many organic molecules are characterized by a low freezing point, high fluidity, and efficient thermal conductivity and are commonly used as thermal energy transfer and heat dissipation media in production. Additionally, precise thermal conductivity in the production process leads to accurate thermal balance calculations, improves the utilization of energy, and reduces production costs. Therefore, determination of accurate thermal conductivity is of significance.^{2,3}

Understanding the mechanism of thermal conduction is fundamental to estimating or designing the efficient thermal conductivities of materials. In recent years, a certain amount of progress has been made in the study of the heat transfer mechanisms of gases,⁴ solids,^{5,6} nanomaterials,^{7,8} and liquid-phase materials.^{9,10} However, many problems still exist in the measurement of thermal conductivity, such as large measurement errors, high time consumption, and special requirements for equipment.¹¹ At the same time, the developed empirical estimation formulas based on different theories and experiences generally have large calculation errors and require other experimental data for calculation.^{12–14} Computational models based on the quantitative structure–property relationship (QSPR) are only suitable for certain organic molecules, making it difficult to satisfy the practical requirements.^{15,16}

In recent years, molecular dynamics (MD) simulation of the liquid heat conduction process and estimation of thermal conductivity has shown important progress.^{17–21} Certain MD

simulations are available for calculating the thermal conductivities of organic molecules, as shown in Table 1. Aldehydes and ketones are widely used in chemical production and daily life, especially in the field of medicine. Therefore, it is important to explore the heat transfer mechanisms of

Table 1. Results of Selected MD Simulations for Calculating Thermal Conductivities of Organic Molecules

authors	method	compounds	deviation (%)	ref
Dysthe et al.	EMD	<i>n</i> -butane, <i>n</i> -decane, <i>n</i> -hexadecane, 2-methylbutane	5–10	22
Zhang et al.	RNEMD	benzene, cyclohexane, water, <i>n</i> -hexane	<7	23
Nieto-Draghi et al.	RNEMD	methylbenzenes	0.2–7.7	24
Matsubara et al.	NEMD	alcohols	≈24	25

Received: February 22, 2020

Published: April 28, 2020

aldehydes and ketones. Currently, simulations for the thermal conductivities of aldehydes and ketones are scarce, and thus this study aims to fill this gap.

The advantage of MD simulations is that they can detect microscopic information (e.g., the microscopic perspective of thermal conduction¹⁰ and the packing fraction^{26,27}) that is difficult to obtain in experiments. Specifically, the heat flux, which is divided into multiple micromodules with corresponding thermal conduction modes, can be used to conveniently explore the contributions of this information and its overall effect.^{28–30} In a liquid-phase system, the heat flux content can be divided into partial heat flux according to different microscopic mechanisms, such as specific interaction between different atoms,^{31,32} chemical structures,^{29,33} and vibration modes.³⁴ In a molecular system, the thermal conduction consists of two components of microscopic thermal energy transfer. One component is transmitted through the movement of molecules produced by kinetic and potential energies, and the other is transferred by atomic interactions, which include bonded and nonbonded interactions.^{9,10,32,35}

In this work, the nonequilibrium molecular dynamics (NEMD) method was adopted to simulate the heat conduction of liquid aldehydes and ketones at different temperatures, and the calculated values and experimental values of thermal conductivity were compared. Moreover, the heat flux was decomposed to calculate the microscopic heat transfer corresponding to each interaction. According to these results, the relationships between multiple microscopic heat conduction models were preliminarily explored, and the contributions of microscopic heat transfer to the thermal conductivities of liquid aldehydes and ketones were investigated.

2. COMPUTATIONAL DETAILS

2.1. Molecules and Potential Models. In this study, two classes of organic molecules were examined, namely, aldehydes and ketones. The thermal conduction of seven linear alkyl aldehydes ranging from butanal to decanal and six linear alkyl ketones ranging from butanone to nonanone in the liquid state was simulated at four different temperatures.

In this paper, the polymer consistent force field (PCFF)³⁶ was used to establish the molecular model of the organic compounds. The potential energy of PCFF can be divided into bonded energy and nonbonded energy. The bonded energy contains the energy of bond stretching, angle bending, torsion, and inversion, and the nonbonded energy includes the energy of Coulomb and 9–6 Lennard-Jones contributions with a cutoff distance of 12.5 Å.

2.2. NEMD Simulation. The heat conduction of organic molecules is simulated by nonequilibrium molecular dynamics (NEMD),^{37,38} as shown as Figure 1.

After the system has relaxed to an equilibrium state, the heat of particles in the heat source increases regularly; i.e., the speed of each particle in the heat source is transformed as follows:

$$v'_s = v_c + \sqrt{1 + \frac{\Delta\varepsilon}{E_k^r}} (v_s - v_c) \quad (1)$$

where v_s is the velocity of particle s in the heat source, v_c is the centroid velocity of the heat source particles, $\Delta\varepsilon$ is a constant equal to the increment of energy in the heat source, and E_k^r is the kinetic energy of particles relative to their center of mass in the heat source.

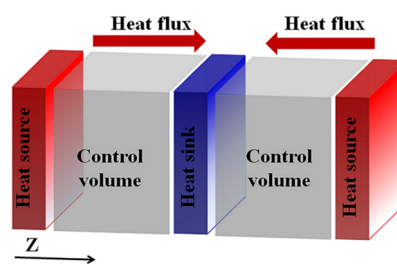


Figure 1. Schematic diagram of NEMD simulation model.

The rate of each particle s in the heat sink is reduced by the following velocity transformation:

$$v'_s = v_c + \sqrt{1 - \frac{\Delta\varepsilon}{E_k^r}} (v_s - v_c) \quad (2)$$

The velocity transformation is performed every Δt , and the heat flux can be calculated based on the heat exchanged, as shown in eq 3. The temperature gradient can be established when the system is stable, and the thermal conductivity is calculated according to Fourier's law, as shown in eq 4.

$$J = \frac{\Delta\varepsilon}{2A\Delta t} \quad (3)$$

$$J = -\lambda(dT/dz) \quad (4)$$

Therefore, A is the cross section of the simulation system perpendicular to the direction of thermal energy transfer, λ represents the thermal conductivity, dT/dz represents the temperature gradient in the z -direction, and the negative sign indicates that the direction of heat conduction is opposite to the temperature gradient direction.

According to the above principle of the NEMD method, the particular simulation steps and parameter settings are described as follows:

1. The software package Materials Studio was used to build the initial configuration of the simulation box. According to the corresponding density of the simulated temperature under actual conditions, the simulated molecules were added into the box such that the lengths of the box in the x -, y -, and z -directions were 27, 27, and 216 Å ($x:y:z = 1:1:8$), respectively. To obtain the temperature profiles, the box was sliced into 40 pieces along the z -direction. Periodic boundary conditions were added in the x -, y -, and z -directions to avoid the surface effect.

2. The simulation was performed by a large-scale atomic/molecular massively parallel simulator (LAMMPS).^{39–45} This version of LAMMPS was modified by Boone et al.⁴⁶ for heat flux calculation. In the simulation process, the systematic potential energy and the force of each particle were calculated using the PCFF.

3. Prior to relaxation, the structure of the system was optimized to minimize the energy of the system.

4. To achieve stability of the simulation system, 140 ps (200 000 steps) of dynamics simulation relaxation were performed under the NPT , NVT , and NVE ensembles to preequilibrium, and 700 ps (1 000 000 steps) of relaxation were performed under the NVT and NVE ensembles to ensure that the structure was equilibrated at the average temperature for which the thermal conductivity is required.

5. After the equilibrium was achieved, the heat conduction was simulated under the NVE ensemble for a total of 2 ns.

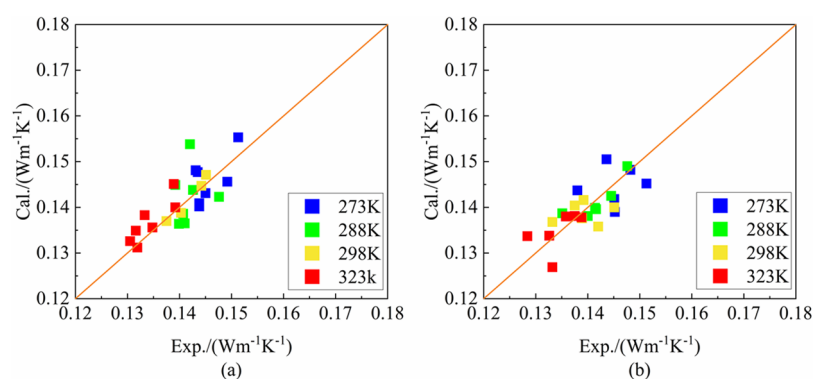


Figure 2. Thermal conductivity values obtained from NEMD simulation versus experimental values of aldehydes (a) and ketones (b).

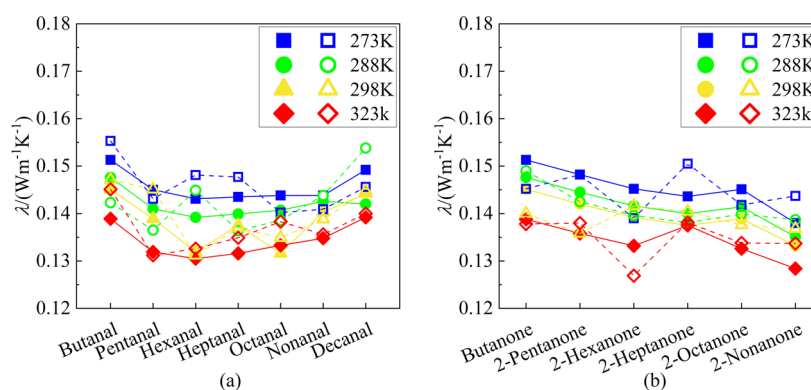


Figure 3. Thermal conductivity values obtained from NEMD simulation compared with experimental values of aldehydes (a) and ketones (b). The solid and dashed lines represent experimental and calculated values, respectively.

According to the asymmetric version of the enhanced heat exchange algorithm,⁴⁷ a constant energy of $\Delta\epsilon = 0.003 \text{ kcal}\cdot\text{mol}^{-1}\cdot\text{fs}^{-1}$ was applied in the heat source and sink in every time step.

Based on the Algaer and Müller-Plathe study,² for a system with a length of several nanometers in the direction of heat transfer and a number of molecules of several hundreds to thousands, the influence of different sizes on the simulation results is not significant. Therefore, we do not check the dependence of different sizes and simulation results.

In the relaxation process, the velocity Verlet method was applied for numerical integration. Because the minimum vibrational period of the H atom is approximately 10 fs, the time step was set to 0.7 fs. The simulation was performed at atmospheric pressure. The temperature and pressure of the system were controlled by a Nosé–Hoover thermostat and barostat,⁴⁸ and the time constants were set to 70 fs and 700 fs, respectively. The Ewald summation was used to calculate the long-range electrostatic interactions. When the heat flux, thermal conductivity, and temperature converged or stabilized, the data were analyzed, and the simulation results were obtained.

2.3. Breakdown of Heat Flux. According to the different interaction, the total heat flux J_{tot} generated by the external energy exchange in the z -direction can be divided into the corresponding partial heat flux, and it includes two main categories: the transport term J_{trans} and the interaction term J_{interact} .^{25,32,33}

$$J_{\text{tot}} = J_{\text{trans}} + J_{\text{interact}} \quad (5)$$

The transport term corresponds to the transmission energy generated by particle migration, which can be divided into kinetic energy J_{kin} and potential energy J_{pot} :

$$J_{\text{trans}} = J_{\text{kin}} + J_{\text{pot}} = \frac{1}{V_{\text{CV}}} \sum_{s \in \text{CV}} \frac{v_s^2}{2m_s} v_{s,z} + \frac{1}{V_{\text{CV}}} \sum_{s \in \text{CV}} U_s v_{s,z} \quad (6)$$

where U_s , m_s , and v_s represent the potential energy, mass, and velocity of atom s , respectively, V_{CV} represents the control volume, and the sum is taken for atoms within the control volume.

The interaction term J_{interact} refers to the heat transfer generated by interatomic forces and its expression is written as follows:^{49,50}

$$\begin{aligned} J_{\text{interact}} &= J_{\text{bond}} + J_{\text{nonbond}} \\ &= J_{\text{str}} + J_{\text{ang}} + J_{\text{tor}} + J_{\text{inv}} + J_{\text{vdW}} + J_{\text{Cl}} \\ &= \frac{1}{V_{\text{CV}}} \sum_X \frac{1}{n} \sum_{s \in X} \sum_{\alpha=1}^{n-1} \sum_{\beta=\alpha+1}^n (f_{X,s,\alpha,s} v_{s,\alpha} - f_{X,s,\beta,s} v_{s,\beta}) (z_{s,\alpha} - z_{s,\beta})^* \end{aligned} \quad (7)$$

where $f_{X,s,\beta,s}$ ($i = \alpha, \beta$) is the n -body force of type X on the atoms. In this paper, the interaction term can be divided into two components: bonded interaction J_{bond} and nonbonded interaction J_{nonbond} . In this formulation, the bonded interaction term J_{bond} consists of four components, J_{str} , J_{ang} , J_{tor} , and J_{inv} , which correspond to bond stretching, angle bending, torsion angle, and inversion angle, respectively. The nonbonded interaction term J_{nonbond} includes two components, J_{vdW} and

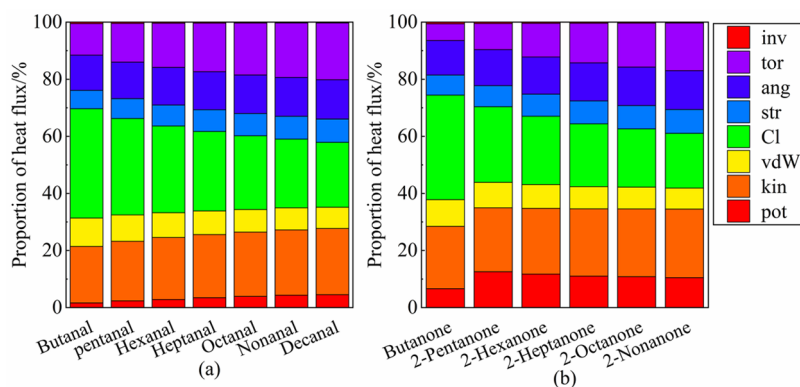


Figure 4. Decomposition of total heat flux into different modes of heat transfer calculated for aldehydes (a) and ketones (b) at 273 K.

J_{Cl} , which are related to the van der Waals and Coulomb interactions, respectively.

Therefore, the heat flux can be divided into eight components: kinetic energy J_{kin} , potential energy J_{pot} , bond stretching J_{str} , angle bending J_{ang} , torsion angle J_{tor} , inversion angle J_{inv} , van der Waals interactions J_{vdW} , and Coulomb interactions J_{Cl} . Similarly, the thermal conductivity λ can also be divided into eight components according to different partial heat fluxes, which is referred to as the partial thermal conductivity obtained by Fourier's law:

$$J_X = -\lambda_X(dT/dz) \quad (8)$$

In addition to the distant atom pair, each interatomic interaction is considered as an atomistic heat path,³³ and thermal energy is transferred by these paths. The partial thermal conductivity of interaction type λ_X equals the path density ρ_X multiplied by the efficiency of heat flux Λ_X as follows:

$$\lambda_X = \rho_X \Lambda_X \quad (9)$$

3. RESULTS AND DISCUSSION

A point-by-point comparison between the calculated values and the experimental values¹ of the thermal conductivities of organic molecules is presented in this section. The thermal conductivity distribution of aldehydes at different temperatures obtained by the NEMD simulation is approximately 0.131–0.155 $\text{W}\cdot\text{m}^{-1}\cdot\text{K}^{-1}$, and the thermal conductivity distribution of ketones at different temperatures is approximately 0.127–0.151 $\text{W}\cdot\text{m}^{-1}\cdot\text{K}^{-1}$, as plotted in Figure 2.

3.1. Thermal Conductivity. Figure 3 plots the NEMD results of the thermal conductivities of two classes of organic molecules: aldehydes and ketones. The corresponding values are listed in Tables S1 and S2. The curves for aldehydes and ketones extracted from experimental values¹ are also included for comparison in each diagram.

The thermal conductivities of the aldehydes first decrease and subsequently increase with molecular chain extension, as shown in Figure 3. This trend is similar to that of ketones. The deviations between the calculated values and the experimental values of the thermal conductivities of aldehydes and ketones are less than 4.32 and 4.86%, respectively, and the average deviation is 2.23%. This observation shows that the thermal conductivity obtained by NEMD simulation is coherent with the experimental value.

Zhang et al.²³ calculated the thermal conductivities of benzene, cyclohexane, *n*-hexane, and other organic com-

pounds, and the deviations between the calculated values and the experimental values were 5.5, 93.5, and 11.7%, respectively. Guevara-Carrion et al.⁵¹ studied the thermal conduction of methanol and ethanol, and the deviations between the calculated thermal conductivities and the experimental values were 4.50 and 17.9%, respectively. Matsubara et al.²⁵ simulated the heat conduction processes of propanol, butanol, octanol, and decanol, and the deviations between the calculated values and the experimental values were 23.7, 26.4, 24.3, and 30.2%, respectively. The deviations of the thermal conductivities of aldehydes and ketones obtained by NEMD simulation in this paper are less than 4.32 and 4.86%, respectively, proving that this work on molecular dynamics simulation is better suited to calculating the thermal conductivities of aldehydes and ketones.

3.2. Breakdown of Heat Flux. According to eqs 5–7, we calculated the heat flux for each interaction. The magnitudes of the partial heat fluxes corresponding to different types of interaction are shown in Figure 4. On average, the interaction term $J_{interact}$ (J_{bond} and $J_{nonbond}$) accounts for 74.8 and 66.4% for aldehydes and ketones, respectively. The transport term J_{trans} (J_{kin} and J_{pot}) accounts for 25.2 and 33.6% for aldehydes and ketones, respectively, on average. Therefore, the interaction term is the main component of total heat flux,⁵² as is the case in alkanes^{28,33} and Lennard-Jones liquid.¹⁰

In the interaction term $J_{interact}$, on average, the bonded interaction term J_{bond} accounts for 37.4 and 33.4% of the total heat flux for aldehydes and ketones, respectively, and the nonbonded interaction term $J_{nonbond}$ of aldehydes and ketones accounts for 37.4 and 33.0%, respectively. This observation means that the heat fluxes of the nonbonded term $J_{nonbond}$ and bonded term J_{bond} are nearly equal.

As shown in Figure 4, J_{ang} and J_{tor} are the dominant components of the heat flux in the bonded term. The ratio of J_{ang} , J_{tor} , and J_{str} is approximately 1.7:2.2:1 for aldehydes on average and is 1.6:1.5:1 for ketones. The J_{Cl} is the major component in the nonbonded term. The Coulomb interaction J_{Cl} is 3.4 times the vdW interaction J_{vdW} for aldehydes on average and is approximately 3.0 times the vdW interaction J_{vdW} for ketones on average.

In the transport term J_{trans} , the kinetic energy J_{kin} is the main component. On average, the kinetic energy J_{kin} is 6.6 times as large as the potential energy term J_{pot} in aldehydes and 2.2 times as large as that in ketones.

Viewed from above, the torsion angle term J_{tor} , angle bending term J_{ang} , Coulomb interaction term J_{Cl} , and kinetic energy term J_{kin} are the major components of the heat

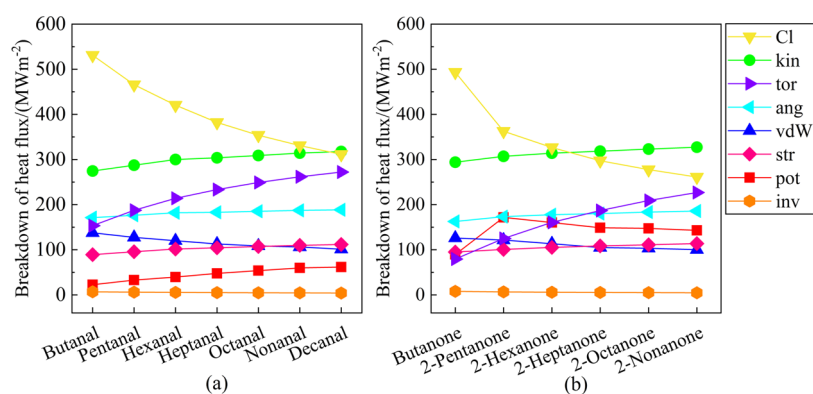


Figure 5. Comparison of heat fluxes of different interactions of aldehydes (a) and ketones (b) at 273 K.

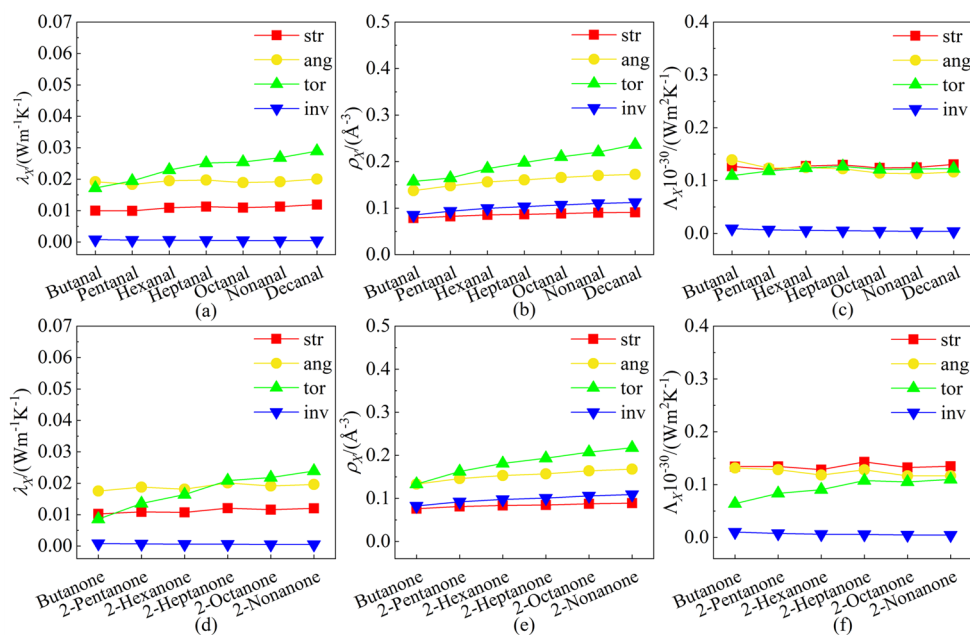


Figure 6. Partial thermal conductivity (λ_X), density (ρ_X), and efficiency (Λ_X) of bond stretching, angle bending, torsion angle, and inversion angle paths for aldehydes (a–c) and ketones (d–f) at 273 K, respectively.

conduction of liquid aldehydes and ketones, showing that the thermal energy is primarily transferred through the vibration of bonding atoms within molecules, Coulomb interaction, and molecular migration.

As shown in Figure 5, as the molecular chain grows, the heat fluxes of the Coulomb interaction J_{Cl} and the vdW interaction J_{vdW} term decrease, and the J_X terms of the other heat fluxes increase. This result indicates that, as the molecular chain grows, the thermal energy transmitted through nonbonded interaction decreases, and the thermal energy transmitted through intramolecular atomic vibration and molecular migration increases. As the molecular volume increases, the probability of intermolecular collision increases, and the heat flux through the kinetic energy term J_{kin} increases. Additionally, the number of intramolecular covalent bonds also increases with the growth of the molecular chain, and thus the bonded interaction terms J_{bond} increase, especially the torsion angle terms J_{tor} . The results of this paper are consistent with those of Matsubara et al.³³ and Ohara et al.²⁸

As shown in Figures 4 and 5, the main proportion of the heat flux gradually changes from the nonbonded interaction term $J_{nonbond}$ to the bonded interaction term J_{bond} as the chain

increases, and the bonded interaction term J_{bond} becomes the dominant component of the total heat flux. We speculate that the main reason for this result is that the force field used in this simulation belongs to the all-atom force field. Even if the molecular framework is small, the degree of freedom of the intramolecular motions is still increasing with the molecular chain length, which means that the proportion of the bonded interaction term J_{bond} is also large, and the proportion of the bonded interaction term J_{bond} and the transport term J_{trans} increases as the molecular chain elongates. In summary, these results indicate that a significant relationship exists between the mechanism of thermal transfer and the molecular structure.⁵³

3.3. Properties of the Atomic Heat Path. The analysis in section 3.2 shows that, with elongation of the molecular chain, the heat flux of the bonded interaction term J_{bond} increases significantly and occupies a dominant portion. Therefore, the contribution of the bonded interaction term J_{bond} to the thermal conductivity is further discussed. Figure 6a–c shows the partial thermal conductivity (λ_X), density (ρ_X), and efficiency (Λ_X) values of the bond stretching, angle bending, torsion angle, and inversion angle paths for aldehydes, and Figure 6d–f shows the same for ketones, respectively.

As shown in Figure 6a, the partial thermal conductivity of the torsion angle λ_{tor} path increases with chain growth for aldehydes, and the partial thermal conductivity attributed to the bond stretching λ_{str} , angle bending λ_{ang} , and inversion angle λ_{inv} paths are slightly different with the increase in the chain. The case is the same case for ketones in Figure 6d.

Figure 6b,e shows the values of the density ρ_X of the heat paths for aldehydes and ketones. The densities of the four types of bonded terms increase with elongation of the molecular chain. As the molecular chain grows, the number of covalent bonds in the simulation system increases, and as shown in Figure 6b,e, all of the path densities increase with the chain growth, and the torsion angle path is especially significant.

As observed from Figure 6c,f, the values of the efficiency of bond stretching Λ_{str} , angle bending Λ_{ang} , torsion angle Λ_{tor} , and inversion angle Λ_{inv} paths fluctuate slightly with the elongation of the chain. For aldehydes and ketones, the efficiency of the torsion angle term Λ_{tor} increases with the growth of the molecular chain, whereas the bond stretching Λ_{str} , angle bending Λ_{ang} , and inversion angle Λ_{inv} paths decrease slightly with the growth of the molecular chain.

Through discussion of the above work, with the elongation of the molecular chain, the number of covalent bonds increases, which makes the proportion of bonded interaction terms J_{bond} increase. Therefore, the partial thermal conductivity of the bonded interaction term J_{bond} also increases. At the same time, the nonbonded interaction term has a great influence on heat transfer, but it decreases with growth of the molecular chain.

4. CONCLUSIONS

1. The thermal conductivity values of the two classes of liquid organic molecules obtained by the NEMD simulation have an average deviation of 2.23% and a deviation of less than 4.86% compared with the experimental values, which indicates that no significant deviation exists between the simulation results and the experimental results.

2. According to the results of heat flux decomposition and the analysis of properties of the atomic heat path, the Coulomb interaction term J_{Cl} , torsion angle term J_{tor} , angle bending J_{ang} , and kinetic energy term J_{kin} play major roles in the heat transfer of liquid aldehydes and ketones.

3. Because the number of covalent bonds in the system increases with the elongation of the molecular chain, the main component of the heat flux gradually changes from the nonbonded interaction term J_{nonbond} (Coulomb interaction term J_{Cl} and vdW interaction term J_{vdW}) to the bonded interaction term J_{bond} (bond stretching term J_{str} , angle bending term J_{ang} , torsion angle term J_{ang} , and inversion angle term J_{inv}). A significant relationship exists between the heat transfer mechanism and the differentiation of the molecular structure.

The NEMD used in this work offers a microscopic perspective of thermal conduction and sheds light on understanding the microscopic heat transfer of liquid organic molecules. Additionally, this study is also helpful in designing efficient thermal energy transfer for liquid materials.

ASSOCIATED CONTENT

Supporting Information

The Supporting Information is available free of charge at <https://pubs.acs.org/doi/10.1021/acs.jcim.0c00184>.

Calculated and experimental values of thermal conductivity at different temperatures and the deviation between them, numerical values of heat flux decomposition, and numerical values of properties of the atomic heat path (PDF)

AUTHOR INFORMATION

Corresponding Authors

Wanqiang Liu – School of Chemistry and Chemical Engineering, Key Laboratory of Theoretical Organic Chemistry and Function Molecule of Ministry of Education, Hunan Province College Key Laboratory of QSAR/QSPR, Hunan Province Key Laboratory of Controllable Preparation and Functional Application of Fine Polymers, Hunan University of Science and Technology, Xiangtan 411201, China; orcid.org/0000-0001-5561-0867; Email: wanqiangliu@hnust.edu.cn

Hu Zhou – School of Chemistry and Chemical Engineering, Key Laboratory of Theoretical Organic Chemistry and Function Molecule of Ministry of Education, Hunan Province College Key Laboratory of QSAR/QSPR, Hunan Province Key Laboratory of Controllable Preparation and Functional Application of Fine Polymers, Hunan University of Science and Technology, Xiangtan 411201, China; orcid.org/0000-0001-8495-6381; Email: zhouhu2006@163.com

Authors

Fan Yang – School of Chemistry and Chemical Engineering, Key Laboratory of Theoretical Organic Chemistry and Function Molecule of Ministry of Education, Hunan Province College Key Laboratory of QSAR/QSPR, Hunan Province Key Laboratory of Controllable Preparation and Functional Application of Fine Polymers, Hunan University of Science and Technology, Xiangtan 411201, China; orcid.org/0000-0002-0818-4137

Haixia Lu – School of Chemistry and Chemical Engineering, Key Laboratory of Theoretical Organic Chemistry and Function Molecule of Ministry of Education, Hunan Province College Key Laboratory of QSAR/QSPR, Hunan Province Key Laboratory of Controllable Preparation and Functional Application of Fine Polymers, Hunan University of Science and Technology, Xiangtan 411201, China; orcid.org/0000-0002-7323-5244

Complete contact information is available at: <https://pubs.acs.org/10.1021/acs.jcim.0c00184>

Funding

W.L. received funding from the National Natural Science Foundation of China (No. 21472040) and the Scientific Research Foundation of Hunan Provincial Education Department, China (Nos. 19K031, 17A065). H.Z. received funding from the National Natural Science Foundation of China (No. 21776067) and the Scientific Research Foundation for Distinguished Young Scholars of Hunan Province, China (No. 2020JJ20013).

Notes

The authors declare no competing financial interest.

ACKNOWLEDGMENTS

The authors thank Xueye Wang's group at Xiangtan University for providing the computing resources. The authors are also grateful to the editor Dr. Zoe Cournia and the reviewers for

comments that have significantly improved the quality of the manuscript.

REFERENCES

- (1) Vargaftik, N. B. *Handbook of Thermal Conductivity of Liquids and Gases*; CRC Press: Boca Raton, FL, 1994.
- (2) Algaer, E. A.; Müller-Plathe, F. Molecular Dynamics Calculations of the Thermal Conductivity of Molecular Liquids, Polymers, and Carbon Nanotubes. *Soft Mater.* **2012**, *10*, 42–80.
- (3) Bao, H.; Chen, J.; Gu, X.; Cao, B. A Review of Simulation Methods in Micro/Nanoscale Heat Conduction. *ES Energy Environ.* **2018**, *1*, 16–55.
- (4) Bird, R. B.; Stewart, W. E.; Lightfoot, E. N. *Transport Phenomena*, 2nd ed.; John Wiley & Sons, Inc.: Hoboken, NJ, 2002.
- (5) Chen, G.; Stokes, H. T.; Esfarjani, K. Heat Transport in Silicon From First-Principles Calculations. *Phys. Rev. B: Condens. Matter Mater. Phys.* **2011**, *84*, 085204.
- (6) Broido, D. A.; Ward, A. Intrinsic Phonon Relaxation Times From First-Principles Studies of the Thermal Conductivities of Si and Ge. *Phys. Rev. B: Condens. Matter Mater. Phys.* **2010**, *81*, 085205.
- (7) Bonini, N.; Rao, R.; Rao, A. M.; Marzari, N.; Menéndez, J. Lattice Anharmonicity in Low-Dimensional Carbon Systems. *Phys. Status Solidi B* **2008**, *245*, 2149–2154.
- (8) Li, W.; Carrete, J.; Mingo, N.; Broido, D. A.; Reinecke, T. L.; Lindsay, L. Phonon Thermal Transport in Strained and Unstrained Graphene From First Principles. *Phys. Rev. B: Condens. Matter Mater. Phys.* **2014**, *89*, 155426.
- (9) Ohara, T. Intermolecular Energy Transfer in Liquid Water and its Contribution to Heat Conduction: A Molecular Dynamics Study. *J. Chem. Phys.* **1999**, *111*, 6492–6500.
- (10) Ohara, T. Contribution of Intermolecular Energy Transfer to Heat Conduction in a Simple Liquid. *J. Chem. Phys.* **1999**, *111*, 9667–9672.
- (11) Assael, M. J.; Antoniadis, K. D.; Wakeham, W. A. Historical Evolution of the Transient Hot-Wire Technique. *Int. J. Thermophys.* **2010**, *31*, 1051–1072.
- (12) Rodenbush, C. M.; Viswanath, D. S.; Hsieh, F. A Group Contribution Method for the Prediction of Thermal Conductivity of Liquids and its Application to the Prandtl Number for Vegetable Oils. *Ind. Eng. Chem. Res.* **1999**, *38*, 4513–4519.
- (13) Nagvekar, M.; Daubert, T. E. A Group Contribution Method for Liquid Thermal Conductivity. *Ind. Eng. Chem. Res.* **1987**, *26*, 1362–1365.
- (14) Tsotsas, E.; Schluender, E. U. Numerical Calculation of the Thermal Conductivity of Two Regular Bidispersed Beds of Spherical Particles. *Comput. Chem. Eng.* **1990**, *14*, 1031–1038.
- (15) Liu, W.; Lu, H.; Cao, C.; Jiao, Y.; Chen, G. An Improved Quantitative Structure Property Relationship Model for Predicting Thermal Conductivity of Liquid Aliphatic Alcohols. *J. Chem. Eng. Data* **2018**, *63*, 4735–4740.
- (16) Lu, H.; Yang, F.; Liu, W.; Yuan, H.; Jiao, Y. A Robust Model for Estimating Thermal Conductivity of Liquid Alkyl Halides. *SAR QSAR Environ. Res.* **2020**, *31*, 73–85.
- (17) Fischer, A.; Smieško, M. Ligand Pathways in Nuclear Receptors. *J. Chem. Inf. Model.* **2019**, *59*, 3100–3109.
- (18) Kang, M.; Chakraborty, K.; Loverde, S. M. Molecular Dynamics Simulations of Supramolecular Anticancer Nanotubes. *J. Chem. Inf. Model.* **2018**, *58*, 1164–1168.
- (19) Lazaridis, T.; Hummer, G. Classical Molecular Dynamics with Mobile Protons. *J. Chem. Inf. Model.* **2017**, *57*, 2833–2845.
- (20) Ru, Q.; Fadda, H. M.; Li, C.; Paul, D.; Khaw, P. T.; Brocchini, S.; Zloh, M. Molecular Dynamic Simulations of Ocular Tablet Dissolution. *J. Chem. Inf. Model.* **2013**, *53*, 3000–3008.
- (21) Alviz-Amador, A.; Galindo-Murillo, R.; Pérez-González, H.; Rodríguez-Cavalló, E.; Vivas-Reyes, R.; Méndez-Cuadro, D. Effect of 4-HNE Modification on ZU5-ANK Domain and the Formation of their Complex with β -Spectrin: A Molecular Dynamics Simulation Study. *J. Chem. Inf. Model.* **2020**, *60*, 805–820.
- (22) Dysthe, D. K.; Fuchs, A. H.; Rousseau, B. Fluid Transport Properties by Equilibrium Molecular Dynamics. III. Evaluation of United Atom Interaction Potential Models for Pure Alkanes. *J. Chem. Phys.* **2000**, *112*, 7581–7590.
- (23) Zhang, M.; Lussetti, E.; de Souza, L. E. S.; Müller-Plathe, F. Thermal Conductivities of Molecular Liquids by Reverse Non-equilibrium Molecular Dynamics. *J. Phys. Chem. B* **2005**, *109*, 15060–15067.
- (24) Nieto-Draghi, C.; Bonnaud, P.; Ungerer, P. Anisotropic United Atom Model Including the Electrostatic Interactions of Methylbenzenes. II. Transport Properties. *J. Phys. Chem. C* **2007**, *111*, 15942–15951.
- (25) Matsubara, H.; Kikugawa, G.; Bessho, T.; Yamashita, S.; Ohara, T. Understanding the Chain Length Dependence of Thermal Conductivity of Liquid Alcohols at 298 K On the Basis of Molecular-Scale Energy Transfer. *Fluid Phase Equilib.* **2017**, *441*, 24–32.
- (26) Heyes, D. M.; Bránka, A. C. The Influence of Potential Softness On the Transport Coefficients of Simple Fluids. *J. Chem. Phys.* **2005**, *122*, 234504.
- (27) Ishii, Y.; Sato, K.; Salanne, M.; Madden, P. A.; Ohtori, N. Thermal Conductivity of Simple Liquids: Origin of Temperature and Packing Fraction Dependences. *J. Chem. Phys.* **2014**, *140*, 114502.
- (28) Ohara, T.; Chia Yuan, T.; Torii, D.; Kikugawa, G.; Kosugi, N. Heat Conduction in Chain Polymer Liquids: Molecular Dynamics Study On the Contributions of Inter- and Intramolecular Energy Transfer. *J. Chem. Phys.* **2011**, *135*, 034507.
- (29) Lin, Y.; Hsiao, P.; Chieng, C. Constructing a Force Interaction Model for Thermal Conductivity Computation Using Molecular Dynamics Simulation: Ethylene Glycol as an Example. *J. Chem. Phys.* **2011**, *134*, 154509.
- (30) Kikugawa, G.; Desai, T. G.; Keblinski, P.; Ohara, T. Effect of Crosslink Formation On Heat Conduction in Amorphous Polymers. *J. Appl. Phys.* **2013**, *114*, 034302.
- (31) Fan, Z.; Pereira, L. F. C.; Wang, H.; Zheng, J.; Donadio, D.; Harju, A. Force and Heat Current Formulas for Many-Body Potentials in Molecular Dynamics Simulations with Applications to Thermal Conductivity Calculations. *Phys. Rev. B: Condens. Matter Mater. Phys.* **2015**, *92*, 094301.
- (32) Torii, D.; Nakano, T.; Ohara, T. Contribution of Inter- and Intramolecular Energy Transfers to Heat Conduction in Liquids. *J. Chem. Phys.* **2008**, *128*, 044504.
- (33) Matsubara, H.; Kikugawa, G.; Bessho, T.; Yamashita, S.; Ohara, T. Effects of Molecular Structure On Microscopic Heat Transport in Chain Polymer Liquids. *J. Chem. Phys.* **2015**, *142*, 164509.
- (34) Lv, W.; Henry, A. Direct Calculation of Modal Contributions to Thermal Conductivity Via Green–Kubo Modal Analysis. *New J. Phys.* **2016**, *18*, 013028.
- (35) Evans, D. J.; Morriss, G. *Statistical Mechanics of Nonequilibrium Liquids*, 3rd ed.; Cambridge University Press: 2008.
- (36) Sun, H.; Mumby, S. J.; Maple, J. R.; Hagler, A. T. An Ab Initio CFF93 All-Atom Force Field for Polycarbonates. *J. Am. Chem. Soc.* **1994**, *116*, 2978–2987.
- (37) Ikeshoji, T.; Hafskjold, B. Non-Equilibrium Molecular Dynamics Calculation of Heat Conduction in Liquid and through Liquid-Gas Interface. *Mol. Phys.* **1994**, *81*, 251–261.
- (38) Jund, P.; Jullien, R. Molecular-Dynamics Calculation of the Thermal Conductivity of Vitreous Silica. *Phys. Rev. B: Condens. Matter Mater. Phys.* **1999**, *59*, 13707.
- (39) Plimpton, S. Fast Parallel Algorithms for Short-Range Molecular Dynamics. *J. Comput. Phys.* **1995**, *117*, 1–19.
- (40) Brown, W. M.; Wang, P.; Plimpton, S. J.; Tharrington, A. N. Implementing Molecular Dynamics On Hybrid High Performance Computers – Short Range Forces. *Comput. Phys. Commun.* **2011**, *182*, 898–911.
- (41) Brown, W. M.; Kohlmeyer, A.; Plimpton, S. J.; Tharrington, A. N. Implementing Molecular Dynamics On Hybrid High Performance Computers – Particle–Particle Particle-Mesh. *Comput. Phys. Commun.* **2012**, *183*, 449–459.

- (42) Brown, W. M.; Yamada, M. Implementing Molecular Dynamics On Hybrid High Performance Computers—Three-body Potentials. *Comput. Phys. Commun.* **2013**, *184*, 2785–2793.
- (43) Nguyen, T. D.; Plimpton, S. J. Accelerating Dissipative Particle Dynamics Simulations for Soft Matter Systems. *Comput. Mater. Sci.* **2015**, *100*, 173–180.
- (44) Nguyen, T. D. GPU-accelerated Tersoff Potentials for Massively Parallel Molecular Dynamics Simulations. *Comput. Phys. Commun.* **2017**, *212*, 113–122.
- (45) Matsubara, H.; Kikugawa, G.; Ohara, T.; Surblys, D. Application of Atomic Stress to Compute Heat Flux Via Molecular Dynamics for Systems with Many-Body Interactions. *Phys. Rev. E: Stat. Phys., Plasmas, Fluids, Relat. Interdiscip. Top.* **2019**, *99*, 051301.
- (46) Boone, P.; Babaei, H.; Wilmer, C. E. Heat Flux for Many-Body Interactions: Corrections to LAMMPS. *J. Chem. Theory Comput.* **2019**, *15*, 5579–5587.
- (47) Wirnsberger, P.; Frenkel, D.; Dellago, C. An Enhanced Version of the Heat Exchange Algorithm with Excellent Energy Conservation Properties. *J. Chem. Phys.* **2015**, *143*, 124104.
- (48) Hoover, W. G. Canonical Dynamics: Equilibrium Phase-Space Distributions. *Phys. Rev. A: At., Mol., Opt. Phys.* **1985**, *31*, 1695–1697.
- (49) Matsubara, H.; Kikugawa, G.; Ishikiriyama, M.; Yamashita, S.; Ohara, T. Microscopic Picture of Heat Conduction in Liquid Ethylene Glycol by Molecular Dynamics Simulation: Difference From the Monohydric Case. *Int. J. Heat Mass Transfer* **2018**, *121*, 1033–1038.
- (50) Matsubara, H.; Kikugawa, G.; Bessho, T.; Yamashita, S.; Ohara, T. Molecular Dynamics Study On the Role of Hydroxyl Groups in Heat Conduction in Liquid Alcohols. *Int. J. Heat Mass Transfer* **2017**, *108*, 749–759.
- (51) Guevara-Carrion, G.; Nieto-Draghi, C.; Vrabec, J.; Hasse, H. Prediction of Transport Properties by Molecular Simulation: Methanol and Ethanol and their Mixture. *J. Phys. Chem. B* **2008**, *112*, 16664–16674.
- (52) Kawagoe, Y.; Surblys, D.; Kikugawa, G.; Ohara, T. Molecular Dynamics Study On Thermal Energy Transfer in Bulk Polyacrylic Acid. *AIP Adv.* **2019**, *9*, 025302.
- (53) Kawagoe, Y.; Surblys, D.; Matsubara, H.; Kikugawa, G.; Ohara, T. Construction of Polydisperse Polymer Model and Investigation of Heat Conduction: A Molecular Dynamics Study of Linear and Branched Polyethylenimine. *Polymer* **2019**, *180*, 121721.